NOISE ESTIMATION IN PANORAMIC X-RAY IMAGES: AN APPLICATION ANALYSIS APPROACH

Peter Michael Goebel[*†], *Ahmed Nabil Belbachir*[‡]

Vienna University of Technology
Pattern Recognition and Image Procesing Group
Favoritenstraße 9/183-2
A-1040 Vienna, Austria.
goe,nabil@prip.tuwien.ac.at

Michael Truppe

Karl Landsteiner Institute
for Biotelematics,
Danube University Krems
Dr.Karl-Dorrek-Strasse 30
A-3500 Krems, Austria
mtruppe@biotelematics.at

ABSTRACT

This paper presents an appropriate approach for the robust estimation of the noise statistics in dental panoramic X-ray images. To achieve maximum image quality after denoising, a new, low order, local adaptive Gaussian Scale Mixture model is presented, which accomplishes nonlinearities from scattering. State of the art methods use multi scale filtering of images to reduce the irrelevant part of information, based on generic estimation of noise. The usual assumption of a distribution of Gaussian and Poisson statistics only lead to overestimation of the noise variance in regions of low intensity (small photon counts), but to underestimation in regions of high intensity and therefore to non-optimal results. The analysis approach is tested on 2000 samples from a database of 50 panoramic X-ray images and the results are cross validated by medical experts. We conclude with a short summary.

Keywords: Noise Estimation, De-noising, Blind Source Separation

1. INTRODUCTION

In medical diagnostics intuitive decisions take place, based on experience, beside the medical knowledge. Therefore, preservation of the overall look of an image, even though after application of an image processing method, is prominent. Appropriate methods have often to deal with detection of small, low contrast image details, situated side by side, differing probably not in gray-level-mean, but may have slightly different variance. Denoising with overestimated noise variance easily remove such details, whereas doing with underestimated, keeps the noise.
Among others, most used methods for image denoising are multi scale filtering based on the wavelet transform [21, 23]. The basic idea is to decompose an image into different contributions in several frequency bands and at different scales, leading to a over complete representation in the transformed space. Thus, the deterministic image content is represented by a set of few strong coefficients, whereas the noise is spread over all coefficients with weakly strength. Therefore, a deconvolution technique is usually applied using linear or non-linear filtering [7, 26, 21] to reduce the contribution of noise in the transformed coefficients. In [20] a combined method for denoising and deblurring is given, using Gaussian Scale Mixtures(GSM).

The works in [3, 4] evaluate the efficiency of denoising and enhancement using simulations of X-ray images contaminated by additive noise of known distribution. Most approaches suppose the noise has Gaussian nature; some suppose a Poisson distribution or a mixture of both distributions. However, X-ray images show neither the Gaussian nor the Poisson distribution alone, because the noise is coherent to the density of matter, consequently the noise variance is spatially adaptive, too. Consider a patient is placed between a X-ray tube, as the source, and a detector of any type. The X-ray tube is operated at a certain *kilo-Voltage-peak* (kVp), which, along with any filtration, determines the energy spectrum of the beam. X-ray photons from the source, which have indeed Poisson counts, are absorbed along the path between the source and detector by the patient's matter (muscle, fat, bone, air, or contrast agents). The photon attenuation of each type of matter depends on its elementary and chemical composition as well as the beam. This effect is quantified by the *mass attenuation coefficients* (MAC), which give the fraction of photons that are absorbed by unit thickness of matter. Unfortunately the MAC is not a con-

*Student Member, IEEE
†fh-campus wien, Course of Studies: Technical Process- and Project Management, Ettenreichgasse 45a A-1100 Wien, Austria
‡Member, IEEE

stant, it varies with the kVp value, because of physical effects of scattering of the photons along its way. For a deeper insight in the basics of the MAC refer to the companion paper of the authors [**?**], where an introduction on scattering is given. Further information about the topic is found in [2, 9].

Therefore, an accurate investigation on the noise model has to be performed for optimal denoising results.
Some attempts of authors to preserve the edges within an image fail in the case of low contrasts. The estimation of noise itself is left open by many authors. A comparative study between six methods is shown in [16]. A method for blind estimation of noise variance is given in [12] and the references herein. Statistical models for images are described in [19] and in [20] the application of Gaussian Scale Mixtures to natural images give very promising results.

2. PROBLEM STATEMENT

The goal is to find better estimates for the noise variance in panoramic X-ray images. The motivation comes from the experience, that the simplifying assumption of *Independently Identically Distributed* (IID) noise statistics may lead to an error in estimation of the noise variances. Thus, in real X-ray images one can find a significant coherence of the noise with the image contents.
To illustrate the problem, two panoramic image acquisitions are depicted: one image (Figure 1) from *Computer Tomography* (CT) scan technique and the other image from X-ray imaging (Figure 2). The CT image (Figure 1) shows an idealistic view of the panoramic X-ray in (Figure 2), which needs to be enhanced and freed from the mixture of noise.

Fig. 1. CT image as a reference, it shows more of the "reali-mage, as the original image is not available.

Fig. 2. An example of the quality of a real panoramic X-ray.

Figure 3 shows the degradation of the image quality if a mixture of Gaussian and Poisson noise is added to the CT image, where the resulting image quality is still far from the real panoramic X-ray image. A classical denoising approach is performed by wavelet coefficients soft-thresholding using an usually noise estimate [7]. The noise is mainly removed, but the image is blurred. Within the weak wavelet coefficients there is hidden edge information, therefore fine details in the image are lost (pseudo-Gibbs phenomenon).

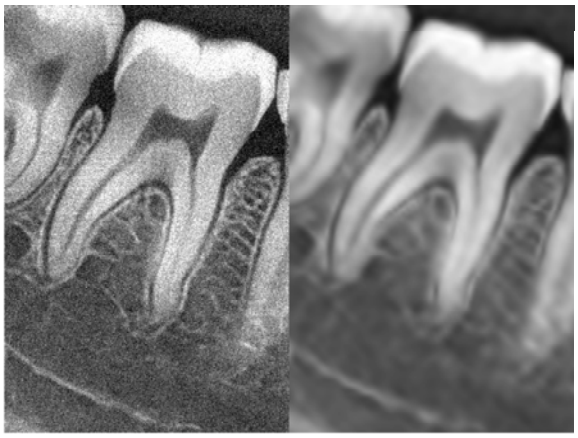

Fig. 3. The zoomed CT image: artificial Gaussian and Poisson Noise added (left); and classically denoised (right).

Figure 4 shows the effect of such a denoising on the real image. The low contrast image (left) is more sensitive than the CT image to the overestimated noise estimate.

The new approach models the X-ray image as a mix-

Fig. 4. A zoom of the real image (left) and it's classically denoised variant (right).

ture of three random sources: a) the background information (BI), b) the information of matter (IOM) and c) the noise. Therefore, one can argue the problem is similar to Blind Source Separation (BSS), where the aim is to reconstruct the noise source, by suppressing the other two.

In this work, a model for estimation of noise is performed, motivated by a comparison between the CT image details and the panoramic X-ray image, which can be exploited for denoising and image enhancement purpose. The new method for estimation of noise is performed with aid of the multi resolution support [22] and is derived from an idea of Blind Source Separation [24] to separate the noise from the image's diagnostic and background information.

3. THE PROPOSED APPROACH

In the proposed approach, prominent constraints are: a) preservation of the image's overall look; b) preservation of the diagnostic content in the image; and c) detection of small, low contrast details in the diagnostic content of the image. As shown in the previous section, state of the art methods provide non-convincing results. The new approach is founded on an attempt to interpret the problem from the view of blind source separation (BSS), thus to see the panoramic image as a sample mixture of (unwanted) background information, diagnostic information and noise. The question is, how to get another sample image? Due to the fixed setup condition of a dental panoramic acquisition system, an empty scan, taken without patient can provide a good another sample - the image of the illuminating background. This background image gives information on the, non-uniform X-ray illumination and also owns the particle statistics, given from the X-ray source, collimation and prefiltration of the beam.

3.1. The Noise Estimation Model

The estimation of the variance of noise is a challenging task, because the usually assumption for the image noise to be independently and identically distributed (i.i.d.) is highly violated. This because of the huge nonlinearity of the radiographic imaging process. To overcome this, Monte Carlo simulations by GEANT4 package [1] were done, thus guided to an simplified, semi-empirical model for generation of the X-ray spectra [5]. Further, a scatter probability model is implemented under some simplifying conditions, which is cross checked with data from the NIST database [9] for verification purpose.

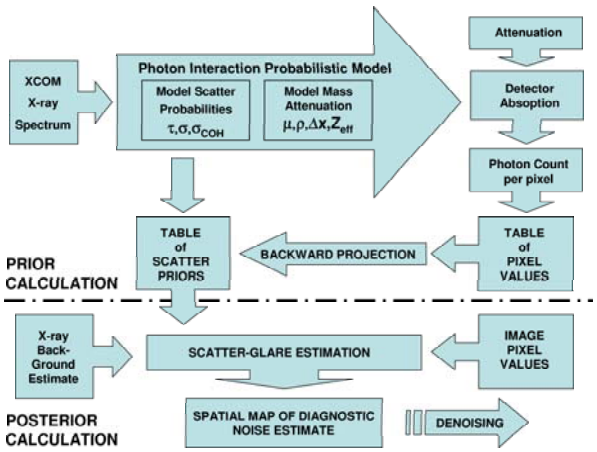

Fig. 5. The Estimation Model has two major parts: the upper is for the calculation of the scatter prior table, whereas the lower part is for the posterior processing of an actual image.

Figure 5 shows an overview on the implemented estimation model. It is subdivided into a prior calculation model and a posterior one. The prior model generates a table of scatter priors, which is then used for the posterior calculation of the spatial noise variance map. For the prior modeling part, the X-ray source energy spectrum is calculated by a semi-empierical model [5]. A probabilistic Photon interaction model is implemented to take the three scattering processes[1] into account.

The simplified probabilistic photon scatter model in Figure 5 models the probabilities per $[cm]$ thickness for scatter interaction in the photon energy range $[8keVto90keV]$, which is suitable for dental panoramic X-ray. Two simplifying assumptions are made: a) Compton scatter σ_{incoh} is assumed to be constant over the diagnostic energy range and effective atomic number Z_{eff}; b) Coherent scatter σ_{coh} is modeled as Rayleigh scatter only and assumed to be independent of Z_{eff}. Finally, in that energy range and range of

[1] i.e. Photoelectric absorption, coherent and Compton scatter

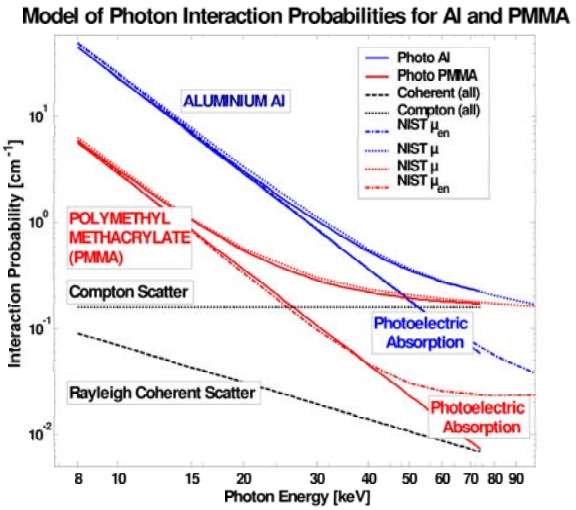

Fig. 6. The simplified Probabilistic Photon Scatter Model.

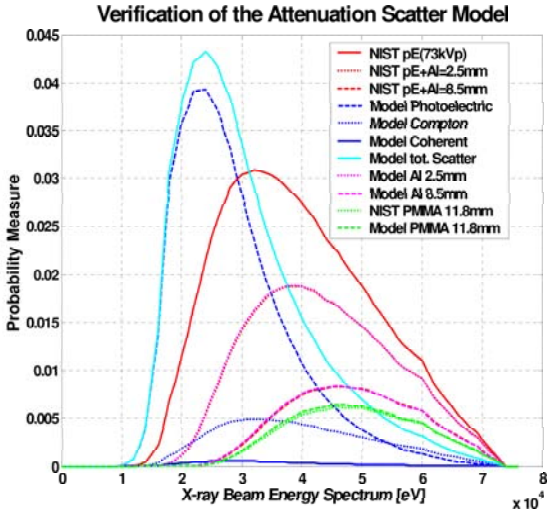

Fig. 7. The Attenuation Scatter Model in Verification.

matter, too, Photoelectric scatter τ varies accordingly to the fraction of $\frac{Z^4}{E^3}$. In Figure 5 the total scattering in terms of the linear attenuation coefficients $\mu = \tau + \sigma_{incoh} + \sigma_{coh}$ for aluminum and PMMA is related to scattering data from the NIST database [9] (dotted lines). Up to $40keV$ the energy mass attenuation coefficients μ_{en} are also in good relation to the modeled Photoelectric absorption τ. Above that point, the model has an upcoming difference, especially at softer matters (i.e. PMMA), but their interaction probability is quite low, thus the error may be neglected. However, the model does not claim to replace any of the Monte Carlo methods [1] in terms of accuracy, but it generates an appropriate enough scatter prior.

The developed model is verified by a physical setup, where the (theoretically) modeled results are compared to practically image pixel values found.

3.2. Physical Setup

Figure 8 defines the physical setup for the verification of the estimation model. At the left hand side, the X-ray generator is shown, which produces the X-ray beam, I_0. A prefiltering stage, Filtration 1 and Filtration 2, by 2.5 mm and 6 mm Aluminum, respectively, attenuates the beam to I_1. The diagnostic absorption by the patient's matter is simulated by Filtration 3 of Poly(Methyl Metracrylate) (PMMA), also called acrylic glass. Finally, filtration by a 3mm lead, which has several holes of 3mm, is essential for the measure of scatter-glare and is only inserted temporally for measurement of that.

The diagnostic image is gathered by an absorbing photo stimulable phosphor (PSP) plate ($BaFBr : Eu^2$), which

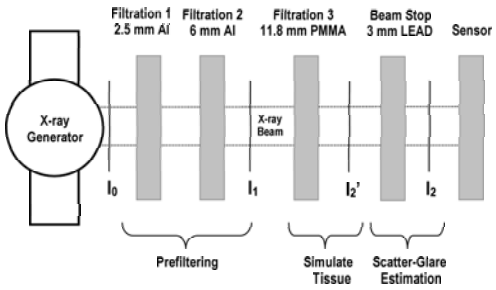

Fig. 8. Physical Setup for the Model

traps and stores the remaining photons. The PSP stored energy is stable until read out off line by an external laser scanner, utilized by the photo stimulated luminescence (PSL) phenomenon. It has high sensitivity, a wide dynamic range of 10^4 to 10^5, and the fluorescence emission is high linearly proportional to the dose in the entire operating range.

Formulating the physical setup of Fig. 8 in mathematical terms of attenuation coefficients leads to:

$$I_2 = \underbrace{\underbrace{I_0 \cdot \exp(-\sum_{i=1}^{K=2}(\mu_{AL}\, d_i))}_{background\ scatter} \cdot \underbrace{\exp(-\mu_P\, d_P)}_{diagnostic\ scatter}}_{I_1} \qquad (1)$$

In (1) the intensity I_2 at the sensor is decomposed into the background part I_1, attenuated by the aluminum filters, at-

tenuated further by the diagnostic part of interest, crossing the primary beam. Within the photon energy range, suitable for dental panoramic X-ray diagnostic, Photoelectric absorption, Coherent scatter and Compton scattering, induce the contrast function of matter [**?**], which forms the image.

Unfortunately an amount of non-negligible noise is produced, stemming from Poisson particle-count statistics, the deflection of the primary X-ray beam caused by the photon interaction with the shell electrons, the grain size of the PSP (5μ), and the PSL read out noise of the laser scanner. In [15] a comparison of image quality of eight different plates is given in terms of presampling modulation transfer function (MTF), normalized Wiener spectra (WSN), and detective quantum efficiency DQE. In section 4, the results in [15] are related to the proposed approach by means of MTF.

$$\mu_p = \frac{\ln\left(\frac{I_2}{I_1}\right)}{d_p} \tag{2}$$

logarithmic fraction

4. THE ANALYSIS AND RESULTS

In the proposed approach the analysis of nature of the given panoramic X-ray images is performed on a large data bank of 2000 samples. A special aluminum phantom was constructed, which supports the ground proof of the analysis. Thus, a collection of several characteristic parameters are maintained. The 3x3 local variance is plotted respectively

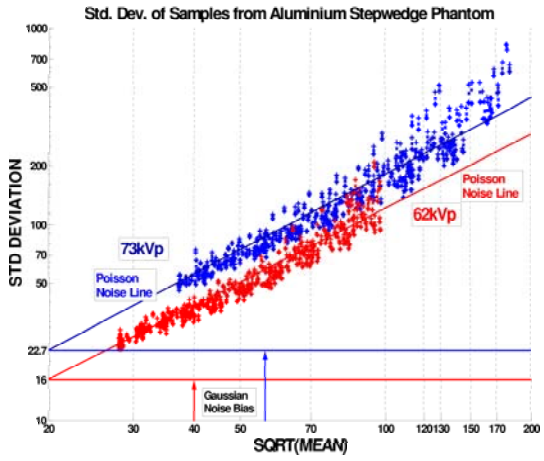

Fig. 9. A Scatter Plot.

to the squared local mean. A slight dependence can be recognized. Then, a plot of the standard deviation over the mean of selected samples is given in Figure 11. Two different operating cases are shown: one at 62 kVp and one at 73 kVp of the X-ray tube. For comparison, the Poisson equivalent dependence is drawn for both cases. The standard deviation of the real image increases from a changing point on. Also the gradient slope of the lower kVp case is higher compared with the other, which is in a good match with interaction theory of photons and matter.

Phenomena of discrete nature are described well by a Poisson distribution [17]. In example, the number of unstable nuclei that decayed within a given period of time in a piece of radioactive substance. The waiting times between such Poisson distributed events are Gamma distributed.

From modeling of multipath fading channels in telecommunication and ultrasonic mammography characterisation of the backscattered echo, a scalable form of a Gamma type distribution, the Nakagami-m desity function is known. The generalized Nakagami density function (GNM) [18] is a type of Gamma density with three free parameters: Ω, m, and s, the scaling factor, the number of free degrees, and an additional shape adjustment parameter, respectively.

Figure 10 shows plots of the GNM for several parameter sets.

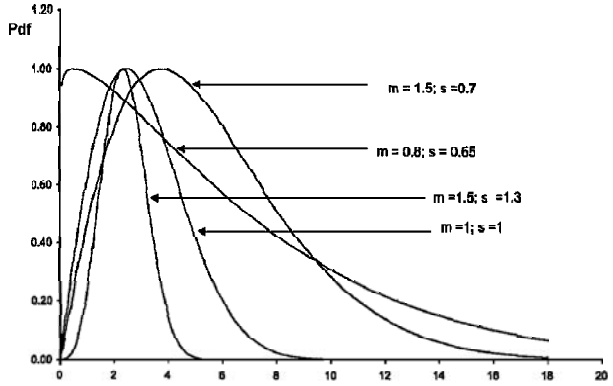

Fig. 10. The Generalized Nakagami-m Density Function (GNM).

The shape adjustment parameter s controls the heaviness of the distribution tail. For $s < 1$ there are heavy tails, which vanish for $s > 1$ to a tight density function. For $m = s = 1$ the GNM becomes the Rayleigh density function; for $m = 1, s \neq 0$ the function becomes the Weilbull density function; and for $m = 1$ and $s = \frac{1}{2}$ it becomes a simple exponential density function. The Generalized Nakagami-m distribution is given by:

$$f(x|m,\Omega,s) = \frac{2s}{\Gamma(m)}\left[\frac{m}{\Omega}\right]^m x^{(2ms-1)} e^{-\frac{m}{\Omega}x^{2s}} \tag{3}$$

The estimation of the density function for the image I_2 is done for the dispersion rather than for the mean values,

motivated from the view, that the Poisson particle rate follows a Gamma distribution. One can argue, that the dispersion, during the exposure for an single image pixel, increases by somewhat function with the number of arriving photons, regardless from what of interaction they stem.

Therefore, a Gamma like density function can be found analyzing the standard deviation (SDEV) of images from flat PMMA and Al phantoms. From the physical setup in Figure 8 several panoramic phantom image scans were made with Filters 1..3. From (1), the local mean and variance of the logarithmic fraction $\mu_p d_p = \ln\left(\frac{I_2}{I_1}\right)$, where the SDEV is shown in Figure 11, once for the unfiltered background I_1 (leftmost curve) and once for I_1, filtered by median filter (rightmost curve). Since there are no interesting details in the background, a kernel size of 9x9 was found to be appropriate to suppress the background noise.

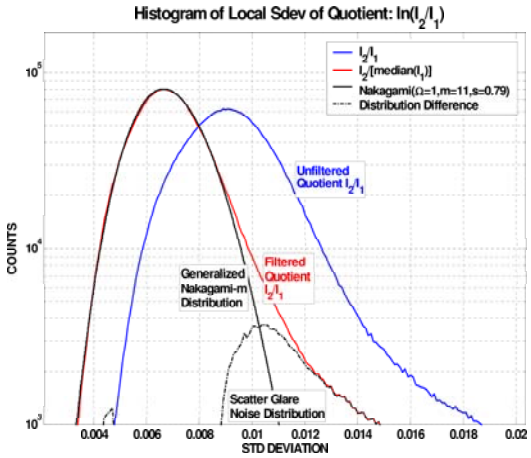

Fig. 11. Image $\sqrt{Var}$ Distribution.

Then a rescaled GNM (3) density function was fitted to the SDEV in Figure 11. The parameters for the density function fits are obtained by maximum likelihood estimation (MLE). Thus, a modified *glmfit* from MATLAB fits a generalized linear model (GLM), calculates the MLE of the mean parameters, and solves the MLE for the shape parameter, which is the reciprocal of the variance parameter. The Nakagami density function best fitted, does not cover the entire heavy tail of the panoramic phantom image SDEV distribution. One can argue, the difference density between the Nakagami model density function and the density function of the acquired image is probably the density of the remaining scatter-glare. To verify this hypothesis, denoted H_0, the scatter-glare was directly measured by a beam stop method (see Figure 8), such that a 3mm lead plate with holes of 3mm diameter is positioned between PMMA filter and detector, too. The image values located surrounding the hole areas, above the attenuation level of the lead screen are then counted accordingly to the scatter-glare distribution.

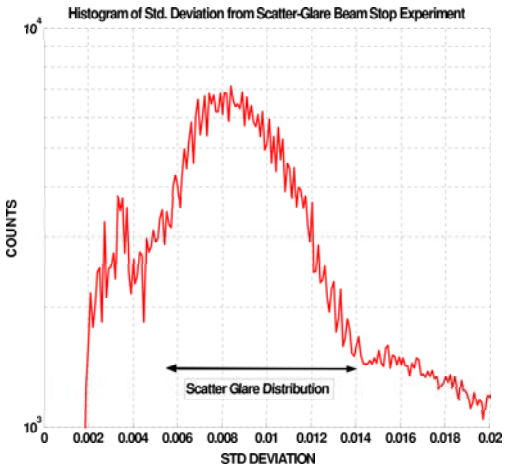

Fig. 12. Scatter-Glare $\sqrt{Var}$ Distribution.

Figure 12 shows a density function from the scatter-glare experiments. Thus this indicates an interestingly result, because the hypothesis seems to be well confirmed. This leads to the support for building a spatial estimate of the diagnostic noise contribution by using the difference density of the SDEV found. Therefore, a spatial noise map of scaled Gaussian random variables is formed as a GSM.

Figure 13 shows an comparison in three images from a MTF phantom: a) source; b) proposed denoising method; c) usually denoising threshold method. At the left hand side, a vertical profile shows the amplitudes of the test sine grating patterns. At the bottom of every image slide shows a zoomed view of the grating with $2.5 lines/mm$. The source a) is noisy, but has sharp contrast; the proposed method b) shows removed noise at very good contrast; finally c) shows

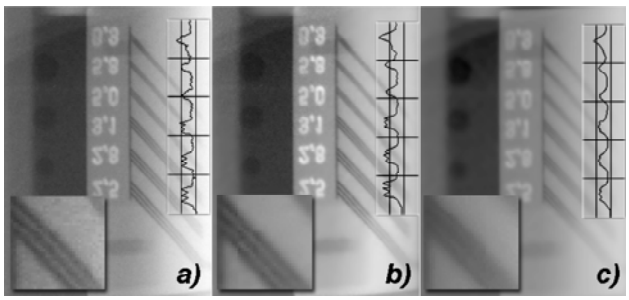

Fig. 13. A comparison of: a) source; b) proposed denoising method; c) usually denoising threshold method.

the noise removed, but the sine grating is heavily distorted. The MTF at $2.5line/mm$ is 51%, 46% and 26% for a), b), c) respectively, where a) is in the same range compared with measurements in [15].

5. CONCLUSIONS

This paper presents a procedure for estimation of the noise in panoramic X-ray images. The local statistics (mean and variance) are calculated from a large database of panoramic X-ray images. A noise model is created, which can be exploited for image enhancement and denoising. The main purpose is to trace the noise model for X-ray image acquisition systems in order to achieve optimal image quality after denoising. The noise model supports the separation of the information of interest by ideas stem from Blind Source Separation. It is shown that the local standard deviation (SDEV) of a PMMA phantom image can be fitted well by a GND, where the heavy tail can be counted for the scatter-glare density. A beam-stop measurement experiment confirms this quantantively. The application of the model to form a Gaussian scale mixture shows promining results for denoising. Further investigations of the success of the method will be published elsewhere.

6. REFERENCES

[1] S. Agostinelli, et al. G4—a simulation toolkit *Nuclear Instruments and Methods in Physics Research Section A: Accelerators, Spectrometers, Detectors and Associated Equipment, Volume 506, Issue 3, 1 July 2003, Pages 250-303.*

[2] Aird EGA. Basic Physics for Medical Imaging. *Heinemann, Oxford, 1988*

[3] M. Analoui. Radiographic Image Enhancement. Part I: Spatial Domain Techniques. *Dentomaxillofacial Radiology, Vol 30, Issue 1 1-9, British Institute of Radiology, 2001*

[4] M. Analoui. Radiographic Image Enhancement. Part II: Transform Domain Techniques. *Dentomaxillofacial Radiology, Vol 30, Issue 2 65-77, British Institute of Radiology, 2001*

[5] J. M. Boone and J. A. Seibert. An accurate method for computer- generating tunsten anode x-ray spectra from 30 to 140 kV. *Medical Physics 24(11) pp.1661-1670, November 1997.*

[6] B. Dannewitz, S. Hassfeld, P. Eckholz, J. Mühling. Effect of dose reduction in digital dental panoramic radiography on image quality. *Dentomaxillofacial Radiology, Vol 31, 50-55, by British Institute of Radiology, 2002*

[7] D.L. Donoho. Denoising by Soft-thresholding. *IEEE Trans. on Information Theory, Vol.41, pp.613-627, 1995*

[8] P.M. Goebel, A. N. Belbachir. An application analysis approach for noise estimation in panoramic X-ray images. Proc. Joint Hungarian-Austrian Conf. Image Proc. and Pattern Recogn. *HACIPPR 2005, Veszprém, Hungary, 11-13 May, 2005: in ISBN 3-85403-192-0 Oesterreichische Computer Gesellschaft*

[9] J. H. Hubbell, S. M. Seltzer Tables of X-Ray Mass Attenuation Coefficients and Mass Energy-Absorption Coefficients (version 1.4). *NISTIR 5632, National Institute of Standards and Technology, Gaithersburg, MD, 1995.*

[10] Lehmann TM, Hiltner H, Handels H. Medizinische Bildverarbeitung. *Lehmann TM (Hrsg): Book for Medical Computer Science 2. Edition Carl Hanser Verlag, Munich 2005*

[11] T. M. Lehmann, E. Troeltsch and K. Spitzer. Image Processing and Enhancement Provided by Commercial Dental Software Programs. *Dentomaxillofacial Radiology, Vol 31, Issue 4 264-272, by British Institute of Radiology, 2002*

[12] P. Meer, J. M. Jolion, A. Rosenfeld. A Fast Parallel Algorithm for Blind Estimation of Noise Variance. *IEEE Trans. on Pattern Analysis and Machine Intelligence, Vol. 12, No. 2, February 1990.*

[13] B. Molander, H-G Gröhndahl and A. Ekestubbe. Quality of film-based and digital panoramic radiography. *Dentomaxillofacial Radiology, Vol 33, 32-36, 2004.*

[14] G. Kaeppler, D. Axmann-Krcmar, I. Reuter, J Meyle and G. Gomez-Roman. A clinical evaluation of some factors affecting image quality in panoramic radiography. *Dentomaxillofacial Radiology, Vol 29, 81-84, 2000.*

[15] Yasushi Nakano et. al. Improved computed radiography image quality from a BaFI:Eu photostimulable phosphor plate *Medical Physics, Vol. 29, No. 4, pp.592-597, April 2002.*

[16] S. I. Olsen. Noise Variance Estimation in Images. *In 8 th Scandinavian Conf. on Image Analysis, Norway, 1993.*

[17] A. Papoulis, U. Pillai Probability, Random Variables, and Stochastic Processes. *4th ed. New York: McGraw-Hill, pp. 103-104, 2002..*

[18] P. M. Shankar. Ultrasonic Tissue Characterisation Using a Generalized Nakagami Model. *IEEE Trans. on Ultrasonics, Ferroelectrics, and Frequency Control, Vol. 48, No. 6, Nov. 2001.*

[19] E. P. Simoncelli. Statistical Models for Images: Compression, Restoration and Synthesis. *Asilomar Conf. on Signals Systems, and Computers, Pacific Grove, CA, Nov. 2-5, 1997.*

[20] J. Portilla, Eero P. Simoncelli. Image Restoration using Gaussian Scale Mixtures in the Wavelet Domain. *9th IEEE Int'l Conf on Image Processing. vol. II, pp. 965-968, Barcelona, Spain. September 2003.*

[21] J.L. Starck, F. Murtagh and A. Bijaoui. Image Processing and Data Analysis: the Multiscale Approach. *Cambridge University Press, 1998.*

[22] J.L. Starck, F. Murtagh Automatic noise estimation from the multiresolution support. *Publ. Astronomic Soc. of the Pacific, 110(744):193-199, 1998.*

[23] JM. Unser, A. Aldroubi and A. Laine. Guest Editorial: Wavelets in Medical Imaging. *IEEE Transactions on Medical Imaging, vol. 22, no. 3, pp. 285-288, March 2003.*

[24] H. Valpola, J. Särela. Accurate, Fast and Stable Denoising Source Separation Algorithms. *Proc. Conf. on ICA and BSS (ICA 2004). Granada, Spain, 22-24 September 2004..*

[25] K. Yoshiura, H. C. Stamatakis, U. Welander, W. D. McDavid, X. Q. Shi, S. Ban, T. Kawazu, M. Tatsumi and S. Kanda. Physical evaluation of a system for direct digital intra-oral radiography based on a charge-coupled device. *Dentomaxillofacial Radiology, Vol 28, Issue 5 277-283, 1999.*

[26] S. Zhong and V. Cherkassky. Image denoising using wavelet thresholding and model selection. *IEEE Int. Conf. on Image processing, Vancouver, BC, Canada, November, 2000.*